

Role of the wall reactor material on the species density distributions in an N₂–O₂ post-discharge for plasma sterilization

K Kutasi¹ and J Loureiro

Centro de Física dos Plasmas, Instituto Superior Técnico, 1049-001 Lisboa, Portugal

E-mail: kutasi@sunserv.kfki.hu

Received 23 May 2007, in final form 11 July 2007

Published 30 August 2007

Online at stacks.iop.org/JPhysD/40/5612

Abstract

The species density distributions in a large post-discharge reactor placed downstream from a flowing microwave discharge in N₂–O₂ are calculated using a three-dimensional hydrodynamic model. The effects of surface losses of N(⁴S) and O(³P) atoms on the density distributions of different species in the reactor are investigated for three different wall materials: (i) Pyrex, (ii) aluminium and (iii) stainless steel. The effects produced by considering different surface loss probabilities corresponding to each one of these materials, as well as by assuming the production of NO from the wall, are evaluated and discussed. The simulation is conducted for the case of a 65 × 25 × 25 cm³ post-discharge reactor fed from a 2450 MHz discharge, at 2 Torr and 2 × 10³ sccm flow rate, in an N₂–xO₂ mixture composition, with x = 0.5–7%.

1. Introduction

The N₂–O₂ post-discharges developed in a large volume reactor are used in many applications, e.g. metal surface cleaning [1], medical sterilization [2, 3], etching and grafting of polymers [4, 5], silicon oxidation [6], thin film synthesis [7] and to increase surface adhesion [8]. Due to its importance the N₂–O₂ post-discharge system has been the subject of many experimental [9–12] and theoretical [11–15] studies carried out in the low-pressure regime. The late-afterglow of a low-pressure N₂–O₂ post-discharge in a remote plasma reactor has been extensively investigated experimentally [16–19]. The densities of N(⁴S) and O(³P) atoms and NO(²Π) molecules have been determined by NO titration at various discharge conditions [3, 16–19], while the UV radiation emitted by the NO(²Π) molecules in the 250–320 nm range (NO_β bands) has been registered in reactors used for medical sterilization [3, 16, 17, 19]. However, whereas the measurements are usually performed in a small experimental reactor made of Pyrex, the applications use larger reactors of metallic walls, e.g. aluminium [20] and stainless steel [3].

Ricard *et al* [16] have realized measurements in two different vessels: a Pyrex and an aluminium one (in fact, this latter is a Pyrex vessel covered with aluminium foil). The measurements have been performed in a 1–2 Torr pressure range and N₂–xO₂ gas mixture compositions with x = 0–20%. In that paper, it has been found that the O-atoms density is higher by a factor of 2 in the aluminium reactor than in the Pyrex, in opposition to the fact that higher atomic surface losses are usually found on metallic surfaces. Concerning now the NO_β bands, in [16] lower intensities have been found in the aluminium vessel, while the dependence of UV emission on the oxygen percentage is different for the two vessels. Whereas two different types of reactors are used in [16], in other investigations only one is usually used and no comparison is presented between data obtained in reactors of different types, see e.g. [2, 17, 20]. Nevertheless, it has been stated in [17] that concerning sterilization achievements, the results are similar in reactors of two different materials. In other experiment, Dilecce and De Benedictis [10] have measured the O-atoms density in a pulsed rf discharge in N₂–O₂, with 10 cm diameter electrodes and 5.5 cm inter-electrode spacing, using either stainless steel electrodes or electrodes covered with Pyrex plates. In [10] it has been found that the O-atoms density is higher by a factor of 2 in the case of Pyrex. Nevertheless, it is worth noting that in [10] the measurements have been realized

¹ Author to whom any correspondence should be addressed. On leave from Research Institute for Solid State Physics and Optics, Hungarian Academy of Sciences, PO Box 49, H-1525 Budapest, Hungary.

in the discharge, so that the surface characteristics in the two experiments are surely quite different.

Owing to the large variety of conditions under which the experiments are realized, namely, regarding the nature of the surface and the shape of the reactor, it is not easy to draw any conclusion about the predicted species densities in the reactor, as well as about their distributions. Most of the experimentally reported atomic densities in the post-discharge reactors are obtained only for a certain position in the reactor and no density distributions for the molecular species are usually given. In spite of this lack of information, from the applications point of view there is a need for the knowledge of the species densities distributions in the reactor, as well as for the predicted modifications introduced by changing the wall materials.

As previously remarked, the aim of this work is to study the modifications introduced by changing the wall materials on the species densities distributions, for both atomic and molecular species, in a large volume post-discharge reactor used in many applications, namely, in medical sterilization and polymer treatments. Here, we investigate the post-discharge of a flowing microwave discharge sustained at the field frequency 2450 MHz, in a 1.3 cm tube radius at 2 Torr gas pressure and 2×10^3 sccm gas flow rate, in an N₂-xO₂ mixture composition with $x = 0.5$ –7%. The species density distributions are calculated for three different wall materials and the modifications introduced by neglecting the surface loss of atoms in Pyrex are also investigated.

2. Model

The species densities in the reactor are calculated with a three-dimensional hydrodynamic model valid for a flowing late-afterglow presented in [21]. The 3D hydrodynamic model is composed of (i) the continuity equations for the different species, (ii) the momentum conservation and (iii) the energy conservation equations. As shown in previous publications [21–23], the species that are still reasonably populated at the entrance of the reactor are the ground-state atoms N(⁴S) and O(³P), the most populated electronically excited states of both gases, which play an important role in the kinetics, N₂(A³Σ_u⁺), O₂(a¹Δ_g) and O₂(b¹Σ_g⁺), and the species NO(X²Π), NO(A²Σ⁺), NO(B²Π), NO₂(X) and O₃. Obviously, both electronic ground-states N₂(X¹Σ_g⁺) and O₂(X³Σ_g⁻) are also considered in the model. The species are not only created in the discharge and carried out by the gas flow to the post-discharge but also produced in the post-discharge itself as a result of the complex interplay kinetics. The charged species are neglected, since they recombine very rapidly in the early afterglow region and their densities at the entrance of the reactor are vanishingly small. The complete set of gas-phase reactions taken into account in the hydrodynamic model has been reported in [21, 22].

The species densities at the reactor entrance are calculated with the help of a self-consistent model for the microwave discharge in N₂-O₂, coupled to the 1D kinetic model of the early afterglow. The discharge model is based on the solutions for the stationary homogeneous electron Boltzmann equation for the microwave field, using the effective field approximation, coupled to a system of rate-balance equations

for the neutral and charged heavy species [23]. The kinetic model is composed of the same rate-balance equations; however, in the afterglow the excitation by electron impact in the system of master equations is cut off. The time-dependent solutions obtained with this latter model constitute the initial conditions for the 3D hydrodynamic model.

In the case of atomic species, besides the gas-phase reactions the surface losses are also considered in the model. With the inclusion of surface processes and taking into account the convective and diffusive transport of species, the continuity equations for the species are written under the form

$$\int_S \rho y_k \mathbf{v} \cdot \mathbf{n} dS - \int_S \nabla(D_k \rho y_k) \cdot \mathbf{n} dS = \int_V m_k S_k^V dV + \int_S m_k S_k^S dS, \quad (1)$$

where ρ denotes the total gas density, \mathbf{v} the gas velocity and \mathbf{n} the unit vector orthogonal to the S surface and directed outwards. Further, y_k denotes the relative mass density ($y_k = \rho_k/\rho$), D_k and m_k are the diffusion coefficient and the mass of the species k , and S_k^V and S_k^S represent the source terms associated with volume and surface reactions, respectively. Since S_k^S represents a term taking into account surface losses, this term is considered in equation (1) only in the last grid point at the proximity of the surface.

The term S_k^V is the sum of the source terms associated with the various gas-phase reactions, which, e.g. for a two body reaction has the form

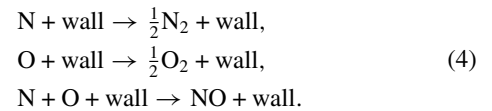
$$S_{k,l}^V = k_{kl} n_k n_l, \quad (2)$$

with k_{kl} denoting the corresponding reaction rate coefficient and n_k and n_l the densities of species k and l involved in this particular reaction, with $n_k = y_k \rho / m_k$. The term for surface loss of the atomic species is calculated using the standard procedure

$$S_k^S = -\gamma_k \frac{v_k}{4} n_k, \quad (3)$$

where $v_k = \sqrt{8k_B T / \pi m_k}$ is the average velocity of k atoms and γ_k is the corresponding atomic surface loss probability.

The losses of atomic species on the wall are attributed to three different elementary processes, which are assumed to be first order [24], and can be written schematically in the form



This list of reactions includes both atomic re-association and NO formation on the wall. These reactions can occur via two mechanisms: Eley–Rideal recombination of a gas-phase atom with a chemisorbed atom and Langmuir–Hinshelwood recombination between a diffusing physisorbed atom and a chemisorbed one. Since we do not consider here a surface kinetic model, it is not possible to decide which mechanism is dominant at the present discharge and surface conditions, for each surface material.

Although it is beyond the scope of this work to consider a detailed surface kinetic analysis, we will attempt to evaluate here the effects produced by assuming NO(X) formation on

Table 1. Measured N-atoms surface recombination probabilities.

Surface	Recombination probability	Conditions	References
Pyrex	2.5×10^{-5}	2 Torr N ₂ dc discharge, $T_s = 300$ K	Gordiets <i>et al</i> [29]
	2×10^{-5}	N ₂ dc flowing afterglow	Ricard <i>et al</i> [30]
	8×10^{-5}	15 mbar N ₂ post-discharge reactor, $T_s = 300$ K	Lefevre <i>et al</i> [31]
	2×10^{-4}	2 Torr N ₂ -2%O ₂ DC discharge	Gordiets <i>et al</i> [29]
	2×10^{-4}	Chosen value for N ₂ -O ₂ mixture	
Aluminium	2.8×10^{-3}	1 Torr N ₂ pulsed RF discharge, $T_g = 300$ K	Adams and Miller [39]
	2.3×10^{-3}	On aluminium-oxide 1 Torr N ₂ post-discharge reactor, $T_s = 300$ K	Sarrette <i>et al</i> [45]
	8.7×10^{-3}	1 Torr N ₂ post-discharge reactor, $T_s = 300$ K	Sarrette <i>et al</i> [45]
	2.3×10^{-3}	Chosen value for N ₂	
	2.3×10^{-2}	Chosen value for N ₂ -O ₂ mixture	
Stainless steel	7.5×10^{-3}	1 Torr N ₂ pulsed RF discharge, $T_g = 300$ K	Adams and Miller [39]
	$7 \times 10^{-2} \pm 0.02$	10–30 mTorr N ₂ RF discharge, $T_s = 320$ –340 K	Singh <i>et al</i> [40]
	6.8×10^{-3}	Chosen value for N ₂	
	6.8×10^{-2}	Chosen value for N ₂ -O ₂ mixture	

the surface onto the species density distributions in the reactor. Thus, due to the difficulty of knowing, based on the data available in the literature, which is the contribution of each of the above mentioned mechanisms to the whole surface loss rate of atoms, we assume here that a fixed α percentage of the N-atoms concentration lost on the surface recombines with an equal O-atoms concentration forming NO molecules. According to this assumption the loss/source terms of different species on the boundary surface, associated with N and O atoms destruction and with NO, N₂ and O₂ creation, are

$$S_N^S = -\gamma_N \frac{v_N}{4} [N], \quad (5)$$

$$S_O^S = -\gamma_O \frac{v_O}{4} [O], \quad (6)$$

$$S_{NO}^S = \alpha(-S_N^S), \quad (7)$$

$$S_{N_2}^S = \frac{1}{2}(1 - \alpha)(-S_N^S), \quad (8)$$

$$S_{O_2}^S = \frac{1}{2}(-S_O^S) - \frac{1}{2}\alpha(-S_N^S). \quad (9)$$

By choosing α in the range 0–1, the effects of NO surface production on the volume density distributions of the various species can then be evaluated.

The surface losses of atomic species depend on many parameters, e.g. type of material, cleanliness, morphology, temperature and surface coverage. In the literature can be found numerous works dealing with the determination of the surface recombination probabilities of atoms (γ probabilities) for different materials: for example, Pyrex [10, 25–38], stainless steel [39–44] and aluminium [39, 41, 44–47]. However, there is quite a large discrepancy between the results obtained by different authors, which could come from a particular surface treatment, the purity of material, surface morphology [48], and surface properties such as crystallinity [49], structure orientation, oxide or nitride type [50]. The differences of several orders of magnitude found in certain cases may also be associated with the employment of different measuring techniques with different measurement errors.

Usually, for determination of γ values it is necessary to measure the atomic density and the surface temperature where the atoms recombine, and to use a kinetic or/and surface model to infer the value of the wall probability. This

latter is determined by fitting the predicted atomic densities obtained from the model with the measured ones. Each model uses certain approximations, which may result in large discrepancies for the derived γ probability. In a gas mixture the problem becomes still more serious due to the convergence of a much more complex kinetics and different surface coverage.

Another source for the discrepancies found are associated with the nature of the medium, i.e. the discharge region where the determinations are made: (i) active discharge region, (ii) time or stationary afterglow, (iii) flowing afterglow and (iv) large post-discharge reactor. In certain cases, even measurements performed on the discharge electrodes are sometimes reported [10, 39]. The surface characteristics may vary a lot from one to another situation, in particular from a surface exposed to ion bombardment to a surface without contact to the plasma.

Here, for the purposes of our study, data determined in the flowing afterglow or, if not available, in a stationary afterglow will be chosen. Since the surface is at room temperature, we attempt to choose loss probabilities data determined under similar conditions. Further, three different wall materials for the reactor will be considered: Pyrex, aluminium and stainless steel. Tables 1 and 2 show the measured γ probabilities, respectively, for recombination of N(⁴S) and O(³P) atoms, used in our discussion, for the above three different wall materials. Information about the discharge or post-discharge regions where the measurements have been realized, the surface or the gas temperature are also indicated.

The surface recombination probabilities of N atoms on a Pyrex surface have been obtained by Gordiets *et al* [29] in pure N₂. These results are in good agreement with the data of Ricard *et al* [30], while Lefevre *et al* [31] have obtained probabilities higher by a factor of 4. Furthermore, Gordiets *et al* [29] have found to exist an increase of γ_N with O₂ addition, although at the lowest O₂ percentages the data obtained at different discharge currents do not reveal a clear tendency. At the lowest discharge current 15 mA used in that paper, it is indicated $\gamma_N = 2.5 \times 10^{-5}$ in pure N₂ and $\simeq 2 \times 10^{-4}$ at 2% of O₂. This latter value is chosen for our investigations.

In the case of aluminium surface, the recombination probability of N atoms in a pure N₂ discharge has been determined by Adams and Miller [39] and Sarrette *et al* [45], at

Table 2. Measured O-atoms surface recombination probabilities.

Surface	Recombination probability	Conditions	References
Pyrex	2×10^{-3}	2 Torr O ₂ dc discharge, $T_s = 300$ K	Gordiets <i>et al</i> [29]
	$(2.0 \pm 0.5) \times 10^{-3}$	Time (stationary) afterglow of 1 Torr O ₂ dc discharge, $T_s = 300$ K	Macko <i>et al</i> [38]
	2×10^{-3}	2 Torr O ₂ pulsed RF discharge, $T_g = 500$ K	Dilecce and De Benedictis [10]
	4×10^{-4}	2 Torr O ₂ -90%N ₂ dc discharge	Gordiets <i>et al</i> [29]
	1×10^{-3}	2 Torr O ₂ -90%N ₂ pulsed RF discharge, $T_g = 500$ K	Dilecce and De Benedictis [10]
Aluminium	4×10^{-4}	Chosen value for N ₂ -O ₂ mixture	
	2×10^{-2}	0.5 mbar O ₂ flowing afterglow, $T_s = 300$ K	Mozetic [47]
	1.5×10^{-2}	0.5 Torr O ₂ RF discharge, $T_s = 400$ -600 K	Gomez <i>et al</i> [41]
	3×10^{-1}	10 mTorr O ₂ discharge, $T_s = 300$ -320 K	Kurucz <i>et al</i> [46]
	1.7×10^{-3}	O ₂ flowing afterglow	Wickramanayaka <i>et al</i> [44]
Stainless steel	2×10^{-2}	Chosen value for N ₂ -O ₂ mixture	
	7×10^{-2}	0.5 mbar O ₂ flowing afterglow, $T_s = 300$ K	Mozetic and Zalar [42]
	2×10^{-2}	0.5 Torr O ₂ RF discharge, $T_s = 400$ -600 K	Gomez <i>et al</i> [41]
	$1.7 \times 10^{-1} \pm 0.02$	10-30 mTorr O ₂ RF discharge, $T_s = 320$ -340 K	Singh <i>et al</i> [40]
	7×10^{-2}	Chosen value for N ₂ -O ₂ mixture	

different pressure values in the 1–5 Torr and 1–16 Torr ranges, respectively. The values obtained by Sarrette *et al* for an oxidized Al surface are in very good agreement with Adams *et al* values, while for pure Al surface the values of Sarrette *et al* are higher by a factor of 3. In the air environment the aluminium is oxidized, so that proper cleaning is needed to take away the oxide layer. Since in a post-discharge reactor the surface is not exposed to ion bombardment, it may be assumed to be oxidized. Accordingly we have interpolated the pressure dependent results of Adams *et al*, getting $\gamma_N = 2.3 \times 10^{-3}$ at 2 Torr, and used this value in our calculations. Finally, for the case of the recombination probability of N atoms in a stainless steel surface, we have chosen again the values determined by Adams and Miller [39], instead of those one order of magnitude higher determined by Singh *et al* [40] at lower pressures. By interpolating the pressure dependent data of Adams *et al* we obtain $\gamma_N = 6.8 \times 10^{-3}$ at 2 Torr.

The data for the recombination probabilities of N atoms in N₂-O₂ mixtures is scarce. The dependence of γ_N as O₂ is added to N₂ gas has been observed in [29] for the case of a Pyrex surface. By fitting the calculated to the measured concentrations of O atoms and NO molecules, in a low-pressure glow discharge in N₂-O₂, at 2 Torr and for the discharge currents of 15, 30 and 80 mA, it has been observed that the probability γ_N increases by one order of magnitude from pure N₂ to 2% of added O₂. Adams and Miller [39] have realized measurements in the case of a boron nitride surface with small O₂ addition, in the range 0.1–0.4%, and they have also found a decrease in the N-atoms density with respect to pure N₂. For the highest percentage 0.4% of O₂, Adams and Miller [39] have measured a surface loss frequency four times higher. On the other hand, Marković *et al* [51] have observed, in the case of a copper surface, that even at a small O₂ admixture, as low as 0.1%, the recombination probability of N atoms increases by one order of magnitude. However, we should keep in mind that the surface recombination probabilities depend, besides the surface properties, also on the relative atomic concentrations near of the wall, due to the competitive adsorption of N and O atoms, see e.g. [29, 52], and this latter strongly depends

on the discharge conditions. Furthermore, in the case of a post-discharge, the probabilities may also vary from the early afterglow to the remote afterglow region due to both the surface characteristics and the mixture composition of the flow gas. Therefore, the surface loss probabilities, determined for a certain gas mixture composition and discharge conditions, may vary considerably from the smaller discharge system, which includes the early afterglow, to the large size flowing-afterglow reactor. Due to these difficulties, it is beyond the scope of this paper to incorporate an elementary surface model. Here, we will just investigate the effects produced in the species density distributions calculated in a large size reactor in N₂-O₂, as the probabilities γ_N are arbitrarily increased by a factor of four and by a factor of 10, relatively to the value measured in pure N₂, as suggested by the above reported experimental observations. The effects of assuming partial NO formation from the wall are also evaluated.

Let us consider now the surface recombination probabilities of O atoms. In the case of a Pyrex surface, the data obtained by Gordiets *et al* [29] in pure O₂ discharges are in good agreement with the values reported by Macko *et al* [38] and Dilecce and De Benedictis [10]. Moreover, Gordiets *et al* [29] have realized measurements also in an O₂-N₂ mixture, in which a sharp decrease has been found for γ_O with small N₂ addition up to 10%. On the contrary, in the range 10–90% of added N₂, the probability γ_O has been found to be independent of the mixture composition. A similar trend has also been observed by Dilecce and De Benedictis [10] in an rf discharge. However, in [10] the surface corresponds to a discharge electrode, which may explain the somewhat higher values found in that paper. Here, we choose from the present discussion $\gamma_O = 4 \times 10^{-4}$.

In the case of other surfaces, the catalytic probe measurements of Mozetic [47] in the flowing afterglow on aluminium allow us to obtain $\gamma_O = 2 \times 10^{-2}$, which is a value somewhat larger than 1.5×10^{-2} determined by Gomez *et al* [41] in an rf ICP discharge. Kurucz *et al* [46] have still measured higher values, but these have been obtained at lower pressure. Since the Mozetic measurements have been realized in the afterglow, we have preferred these data.

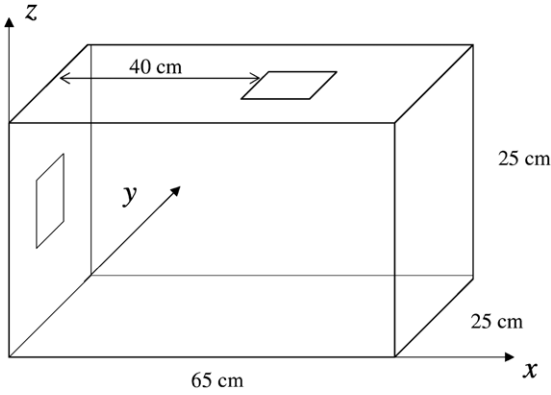


Figure 1. Post-discharge chamber used in the simulation.

Finally, the probability $\gamma_{\text{O}} = 7 \times 10^{-2}$, measured by Mozetic and Zalar [42] for a stainless steel surface using a catalytic probe in flowing afterglow, has been chosen, in contrast to the measurements performed by Gomez *et al* [41] and Singh *et al* [40] in rf discharges.

Contrary to a Pyrex surface, where a dependence of γ_{O} with N_2 addition has been observed [10, 29], Dilecce and De Benedictis [10] have not detected any variation for the case of a stainless steel surface, which may suggest that the recombination probabilities in $\text{O}_2\text{-N}_2$ do not differ so much from pure O_2 . In aluminium there are no measurements in mixtures, so we will assume that both metallic surfaces behave similarly presenting vanishingly small modifications for γ_{O} , as N_2 is added to O_2 into the discharge.

In the conditions of the system we want to model, the active species are firstly created in an $\text{N}_2\text{-O}_2$ microwave flowing discharge and after they pass through a short afterglow tube, with the same inner radius as the discharge, they are then expanded into the post-discharge reactor presented in figure 1. This chamber is similar to the one used by Philip *et al* [17] in their experiments. However for modelling convenience, we consider the gas outlet on the top plane instead of the bottom. From the fluid dynamics point of view there is no difference if the exit is on the top or on the bottom, since the gravity force at these densities does not play any role. The size of the reactor is $65 \times 25 \times 25 \text{ cm}^3$. The entrance is situated on the west plane at a distance of 8 cm from the top. The $2.6 \times 2.6 \text{ cm}^2$ square inlet and outlet are symmetrically positioned on the west and top walls, respectively, so that only one-half of the chamber needs to be considered for the simulation. In the connecting zone between the discharge and post-discharge reactor (not shown in figure 1) we consider 1 ms for the species flight-time, which under present conditions of 2 Torr and 2×10^3 sccm gas flow rate corresponds to a distance of approximately 4 cm (see [21, 22]).

3. Results and discussion

3.1. Influence of the assumed surface recombination probabilities

Let us start by analysing the influence of increasing the N-atoms surface recombination probability, as O_2 is added to N_2 gas, on the predicted concentrations of $\text{N}(^4\text{S})$ and $\text{O}(^3\text{P})$

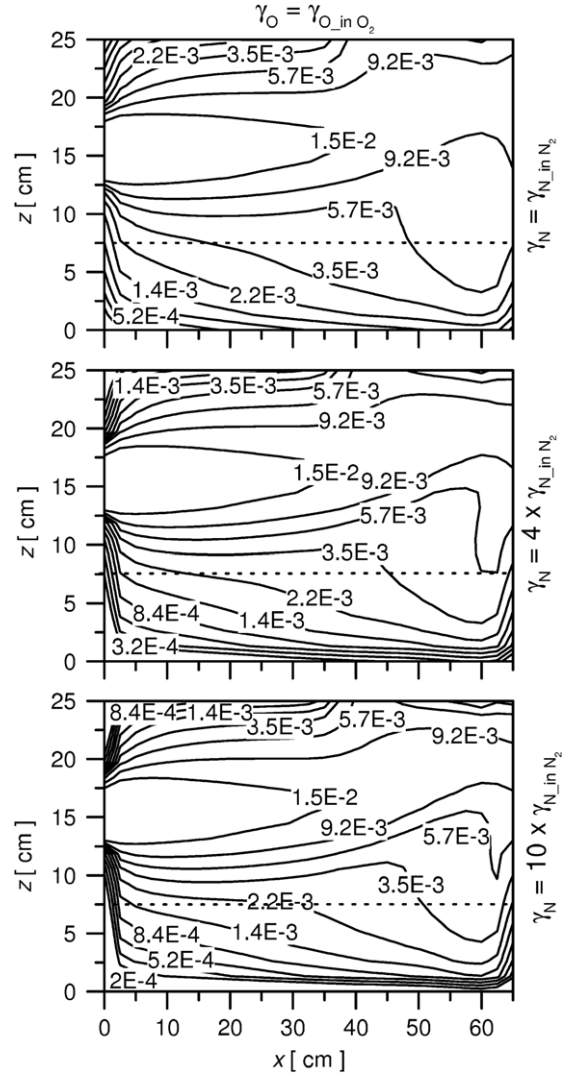


Figure 2. Relative density distributions of $\text{N}(^4\text{S})$ atoms in the $x\text{-}z$ vertical plane at $y = 12.5 \text{ cm}$ in a stainless steel reactor, for the following γ_{N} values: (i) 6.8×10^{-3} (upper); (ii) $4 \times 6.8 \times 10^{-3}$ (middle); (iii) $10 \times 6.8 \times 10^{-3}$ (lower). These concentrations are obtained in a post-discharge from a 2450 MHz flowing microwave discharge at 2 Torr and 2×10^3 sccm gas flow rate, in an $\text{N}_2\text{-}2\%\text{O}_2$ mixture.

atoms. The calculations are carried out for the post-discharge of a 2450 MHz flowing microwave nitrogen discharge at 2 Torr and 2×10^3 sccm gas flow rate, for 2% of added O_2 , and in the case of a stainless steel reactor. As discussed above, this corresponds to the case where the surface recombination probabilities γ_{N} are the largest. Also as discussed in the previous section, we consider here three different values for γ_{N} as follows: (i) 6.8×10^{-3} (that is the value in pure N_2), (ii) $4 \times 6.8 \times 10^{-3}$ and (iii) $10 \times 6.8 \times 10^{-3}$. Concerning the recombination probability for O atoms, this is assumed with the same value as in pure O_2 , 7×10^{-2} , due to the reasons discussed above. Figure 2 shows the relative density distribution of N atoms, in the $x\text{-}z$ vertical plane at $y = 12.5 \text{ cm}$. With an increase in the probability γ_{N} , from its value in pure N_2 to a four times larger value, we observe a decrease in $\text{N}(^4\text{S})$ density near the wall by a factor of about 1.5. As a further increase of γ_{N} is considered by a factor of 10, the N-atoms

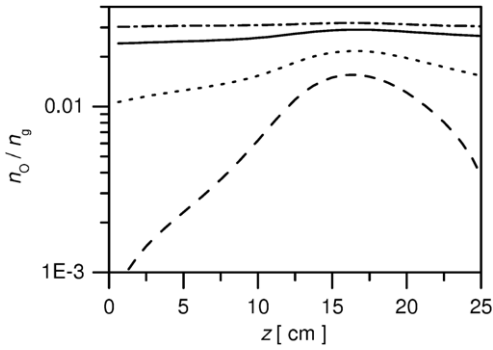


Figure 3. Relative density distributions of O(³P) atoms as a function of z coordinate at $(x, y) = (32.5 \text{ cm}, 12.5 \text{ cm})$, for the same discharge conditions as in figure 2 and for the following cases: (i) Pyrex (—), (ii) aluminium (- - -), (iii) aluminium using $\gamma_{\text{O}} \times 10^{-1}$ (·····) and (iv) aluminium using $\gamma_{\text{O}} \times 10^{-2}$ (- · - ·).

density still decreases by another factor of 1.5. In the bulk of the reactor, e.g. at 7.5 cm from the bottom wall, the N-atoms density decreases by a factor of 1.6 when the probability γ_{N} increases from 6.8×10^{-3} to $10 \times 6.8 \times 10^{-3}$. On the other hand, no density alteration has been observed for the O atoms as a result of the changes in the probability γ_{N} . In line with the data of Marković *et al* [51], we will choose in the following analysis of this paper the probabilities γ_{N} in pure N₂ multiplied by a factor of 10 for aluminium and stainless steel surfaces, which correspond to their maxima values.

As referred in section 1, the measurements of Ricard *et al* [16] show a higher density of O(³P) atoms in an aluminium reactor than in Pyrex. For such higher concentrations in aluminium the surface loss probability γ_{O} should be considerably lower than in Pyrex, even lower than that determined in N₂-O₂ mixtures. Figure 3 shows the O-atoms relative density as a function of the vertical z coordinate at the point $(x, y) = (32.5 \text{ cm}, 12.5 \text{ cm})$, which is in the middle of the reactor, for the following cases: (i) Pyrex, (ii) aluminium with $\gamma_{\text{O}} = 2 \times 10^{-2}$, (iii) aluminium with a probability γ_{O} one order of magnitude lower and (iv) aluminium with γ_{O} two orders of magnitude lower. It is worth noting at this point that the γ_{O} values in Pyrex are 2×10^{-3} and 4×10^{-4} in pure O₂ and in an N₂-2%O₂ mixture, respectively. Figure 3 shows that the relative density of O atoms in aluminium gradually increases with the decrease in γ_{O} . As this probability is multiplied by a factor of 10^{-2} relatively to the value 2×10^{-2} in pure O₂, the density becomes larger by a factor of 1.2 than that obtained in Pyrex, which is close to the experimental ratio of 2 reported in [16].

Figure 4 shows the relative NO(²Π) density, for the same conditions as in the previous figure, also as a function of the z coordinate in the middle of the reactor. At $z = 5 \text{ cm}$ a difference of approximately the same order is found between the densities obtained in Pyrex and in aluminium, as $\gamma_{\text{O}} = 10^{-2} \times 2 \times 10^{-2}$ is assumed for this latter, as in the case of the measurements reported in [16].

The reduction of γ_{O} probability down to 2×10^{-4} in aluminium surfaces allows us to reproduce the experimentally observed trends of O and NO(²Π) densities in [16]; however, there is no other evidence supporting such a high diminution of the surface loss probability of O atoms. To our knowledge the lowest γ_{O} probability equal to 1.7×10^{-3} has been measured by

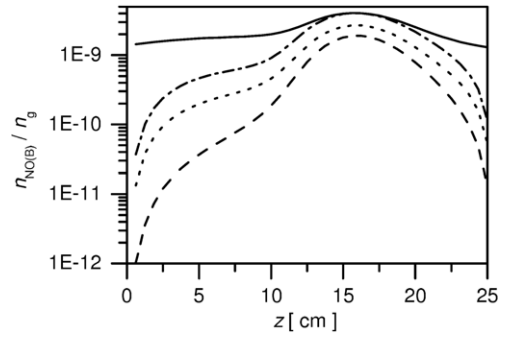


Figure 4. Relative density distributions of NO(²Π) as a function of z coordinate at $(x, y) = (32.5 \text{ cm}, 12.5 \text{ cm})$, for the same discharge conditions as in figure 2 and for the following cases: (i) Pyrex (—), (ii) aluminium (- - -), (iii) aluminium using $\gamma_{\text{O}} \times 10^{-1}$ (·····) and (iv) aluminium using $\gamma_{\text{O}} \times 10^{-2}$ (- · - ·).

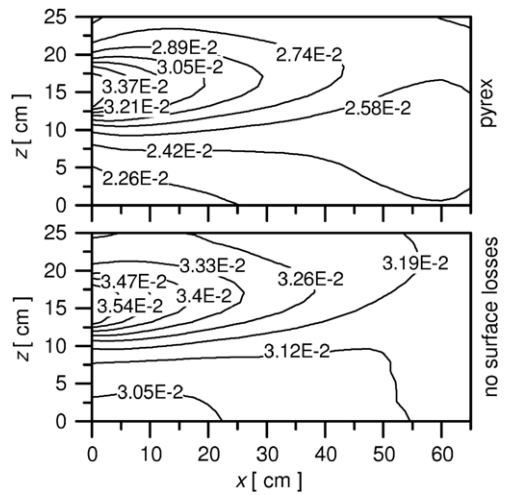


Figure 5. Relative density distributions of O(³P) atoms in the x - z vertical plane at $y = 12.5 \text{ cm}$ in the case of a Pyrex reactor (upper) and when the surface losses are not included in the model (lower).

Wickramanayaka *et al* [44] on mechanically and chemically polished aluminium surfaces, but this value is still larger by one order of magnitude than the value we have needed to assume in this paper. We note that in the case of Pyrex surface, in which the probability γ_{O} has been determined for different N₂-O₂ mixture compositions, a factor of 5 has been found between the situations of pure O₂ and the mixture, presenting this latter the smallest value. We further note that in the case of the experiments performed by Ricard *et al* [16] aluminium foil has been used, whose surface structure is probably different from the aluminium used for reactor building. According to these observations, the results obtained using aluminium foil cannot probably be used to draw conclusions for an aluminium reactor.

To conclude let us consider now the situation where the surface losses in the reactor are simply neglected. Figure 5 shows for comparison the O-atoms density distribution in the x - z vertical plane at $y = 12.5 \text{ cm}$, for Pyrex surface, with $\gamma_{\text{O}} = 4 \times 10^{-4}$ and $\gamma_{\text{N}} = 2 \times 10^{-4}$, and when the surface losses are ruled out from the model. In this latter case the density grows up to 20% larger and this difference remains almost constant in the whole reactor. In the case of the other species no significant changes are observed.

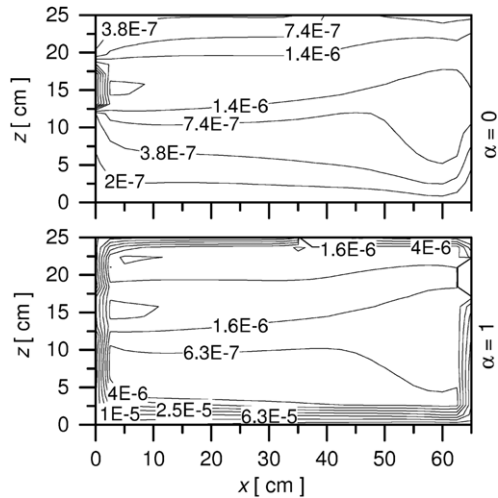


Figure 6. Relative density distribution of NO(X) in the x - z vertical plane at $y = 12.5$ cm when all $N(^4S)$ atoms lost on the surface of a stainless steel reactor ($\gamma_N = 6.8 \times 10^{-2}$ and $\gamma_O = 7 \times 10^{-2}$) are recombined into N_2 (upper, $\alpha = 0$ see text) or transformed into NO molecules (lower, $\alpha = 1$).

3.2. NO surface production

In this section we evaluate the influence of NO surface production in increasing the NO(X) concentration in the reactor. We present the results obtained for an N_2 -2% O_2 initial mixture composition in a stainless steel reactor, case where the atomic loss probabilities have their highest values $\gamma_N = 6.8 \times 10^{-2}$ and $\gamma_O = 7 \times 10^{-2}$. Figure 6 shows the relative density distribution of NO(X) molecules in the x - z vertical plane at $y = 12.5$ cm (that is in the middle plane) for the extreme cases in which all N atoms that have been lost on the metallic surface either recombine into N_2 molecules or they re-associate with adsorbed O atoms to form NO(X) molecules. These situations correspond to values of the α parameter equal to 0 and 1, respectively, as stated in equations (7)–(9). In this latter case the concentration of O atoms is obviously in excess relatively to that of N atoms in order to verify the inequality $(-S_O^S) > (-S_N^S)$ in equation (9). From figure 6 we observe that even in the case $\alpha = 1$, the source of NO(X) coming from the surface does not produce significant changes in the volume density distribution of NO(X), except in a narrow 5 cm width zone near the wall. This is a consequence of the fast volume dissociation reaction for NO(X) due to collisions with $N(^4S)$ atoms, $NO(X) + N(^4S) \rightarrow N_2(X, v \simeq 3) + O(^3P)$, leading to $O(^3P)$ formation [23], which prevents that NO(X) may be produced.

By inspection of figure 6 we observe that the increase in NO(X) concentration due to surface production of this species is much larger in zones of the reactor with lower N-atoms density (see figure 2), since NO(X) is strongly destroyed in collisions with atomic nitrogen. That is the case of the chamber corner $(x, z) = (0-5 \text{ cm}, 0-5 \text{ cm})$. Figure 7 shows for completeness the relative density distribution of NO(X) molecules in this limited x - z vertical plane near the corner at $y = 12.5$ cm, in the case of a stainless steel reactor, for different α values equal to 0, 0.25, 0.5 and 1. This figure shows that within 4 cm distant from the wall, the NO(X) density reaches approximately the same value independently of the α value we assume.

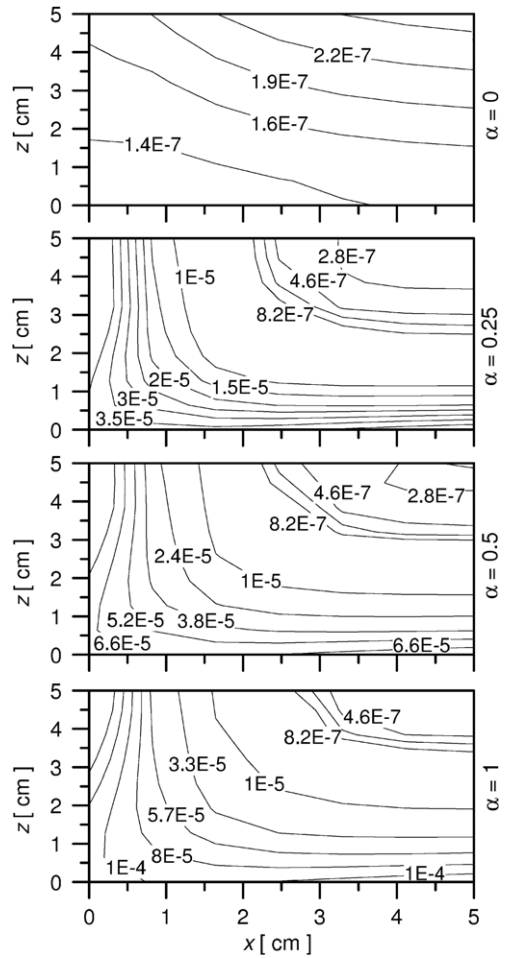


Figure 7. Relative density distribution of NO(X) in the chamber corner of the x - z vertical plane, with both coordinates varying only in the 0–5 cm interval, at $y = 12.5$ cm, in the case of a stainless steel reactor (as in figure 6), for the following α values: 0, 0.25, 0.5 and 1 (from the upper to the lower).

3.3. Species densities in reactors of different wall materials

In this section we compare the different species density distributions obtained in reactors of different wall materials for the case of a post-discharge from a discharge realized in an N_2 -2% O_2 initial mixture composition. The surface recombination probabilities of N atoms on aluminium and stainless steel are $\gamma_N = 2.3 \times 10^{-2}$ and 6.8×10^{-2} , respectively, while for O atoms we have $\gamma_O = 2 \times 10^{-2}$ and 7×10^{-2} . Here, we assume that 50% of $N(^4S)$ atoms lost on the wall are re-associated with adsorbed O atoms forming NO(X) molecules on the wall or, which is the same for this purpose, that 50% of N atoms adsorbed on the wall re-associate with O atoms coming from the gas-phase forming NO(X) on the wall. Both situations correspond to $\alpha = 0.5$ in our model. Our choice to $\alpha = 0.5$ can be supported in part by the Nasuti *et al* [52] model calculations; however, as shown in the previous section, the surface production of NO(X) introduces only minor modifications on the density distribution of this species in the central part of the reactor.

Nasuti *et al* [52] have developed a single-species surface model in the case of hypersonic flows to predict catalytic recombination rates of O and N atoms on silica re-entry thermal

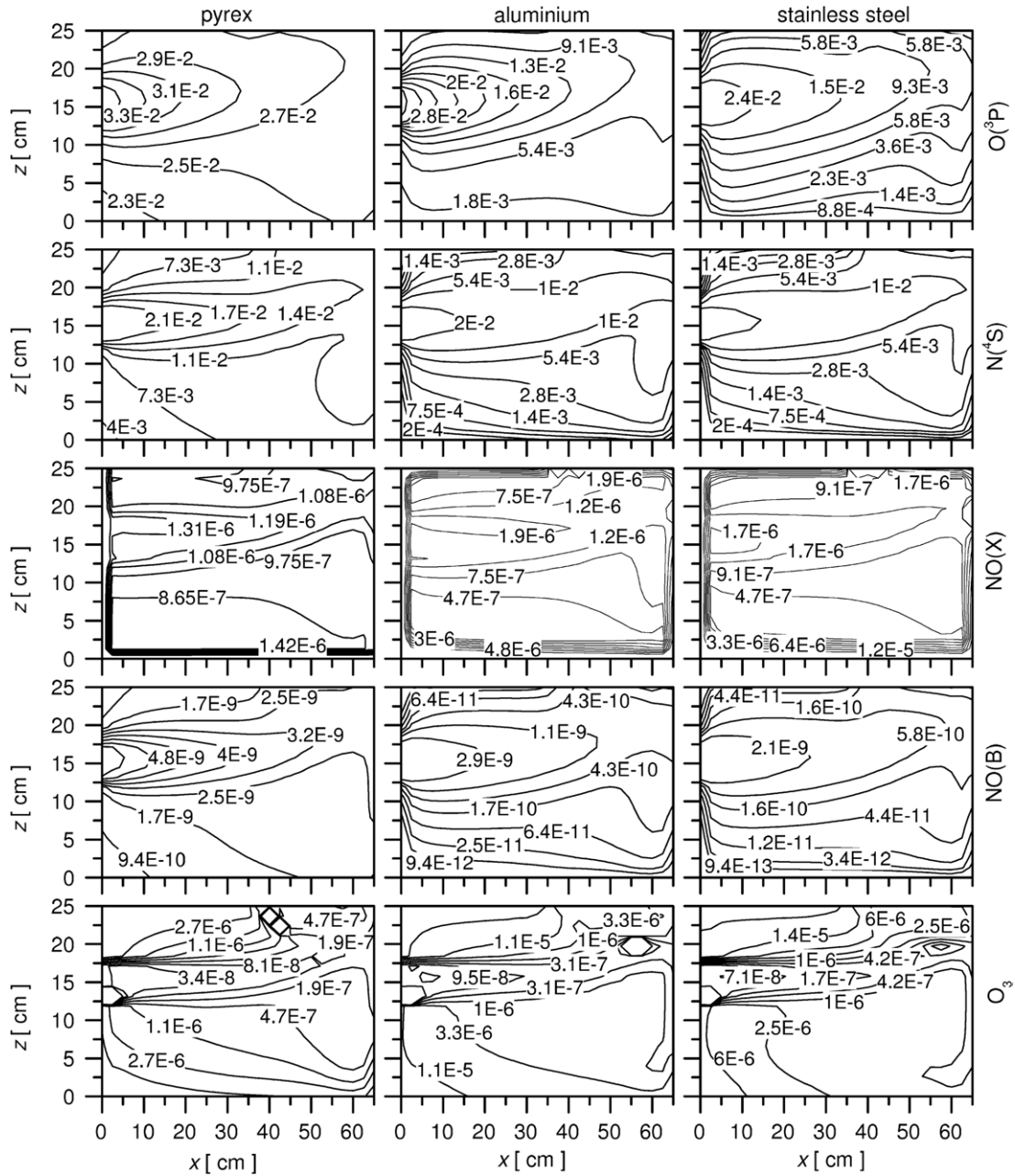


Figure 8. Relative density distributions, in the x - z vertical plane at $y = 12.5$ cm, for the following species from rows 1 to 5 by order: O(³P), N(⁴S), NO(X), NO(B) and O₃. Columns 1 to 3 are for Pyrex, aluminium and stainless steel. The calculations are for 2 Torr, 2×10^3 sccm gas flow rate and N₂-2%O₂ mixture composition.

protections. In their conditions of spacecraft re-entry the molecular gas is fully dissociated. The model determines four different recombination probabilities for O and N atoms: γ_{OO} , γ_{NN} , γ_{ON} and γ_{NO} , which define the percentages of the total atomic rate that recombine under the form of N₂, O₂ and NO. According to their calculations, when the oxygen to nitrogen atomic density ratio is of the order of 10, the N atoms re-associate preferentially as NO molecules ($\approx 90\%$). In our case although the initial mixture composition is preferentially constituted by molecular nitrogen, the atomic concentration of O atoms is clearly dominant with the ratio [O]/[N] varying in the range 4–10. This may suggest that in our case, depending on the atomic density ratio, the α value should be lower

than 0.9. The value assumed here of $\alpha = 0.5$ may be seen hence as a somewhat averaged value for the conditions under analysis in this paper.

Figure 8 shows for the above mentioned conditions (2 Torr pressure, 2×10^3 sccm gas flow rate and N₂-2%O₂ mixture composition), the relative density distributions of various species, in the x - z vertical plane at $y = 12.5$ cm, for three wall materials as follows: Pyrex (first column), aluminium (second column) and stainless steel (third column). The species from the top to the bottom row are by order: O(³P), N(⁴S), NO(X ²Π), NO(B ²Π) and O₃.

The relative densities of O(³P) atoms are shown in the first row of figure 8. In the case of a Pyrex reactor the O-atoms

density decreases for about 30% from the reactor's entrance to the bottom plane, while in the case of aluminium and stainless steel reactors these decreases are by more than one order of magnitude. Comparing with the Pyrex reactor, the density is lower in the aluminium with a factor varying between 1.5 and 10, depending on the position in the reactor. In the flow direction the largest difference is a factor of 5 at the east plane, while the most pronounced difference occurs in a 5 cm width zone near the bottom. In the stainless steel these densities are still lower than in aluminium, since the surface loss probability is higher. At the east plane the O-atoms density is a factor of 7 lower than in Pyrex, while near the bottom plane the density difference is 25.

In the case of the relative density of $N(^4S)$ atoms, the changes from one to another material are slightly less pronounced than with $O(^3P)$ atoms, see the second row of figure 8. While the O-atoms density in the flow direction in aluminium is lower by a factor of 5 than in Pyrex, the corresponding reduction for N atoms is just ≈ 1.2 . Since the volume loss of N atoms in the reactor is mainly due to the reaction $N(^4S) + O(^3P) + N_2 \rightarrow NO(X) + N_2$ and the density of O atoms decreases from Pyrex to aluminium, the rate of N-atoms volume losses also decreases. Thus, the increase of the surface loss rate from Pyrex to aluminium is partially compensated by a reduction of volume loss rate, both producing an overall reduction of N-atoms density, but by a smaller extent than could be predicted from the increase in γ_N probability. At the bottom plane near the west plane, the reduction of N-atoms density is about one order of magnitude from Pyrex to aluminium. In the case of stainless steel slightly lower densities are still found as compared with aluminium, mainly in a 10 cm width zone near the bottom plane.

The $NO(X^2\Pi)$ density distributions are presented in the third row of figure 8. As mentioned above, these results are obtained assuming $\alpha = 0.5$, that is assuming that 50% of the N atoms lost on the wall are re-associated with $NO(X)$ molecules. In aluminium the $NO(X)$ density is slightly lower than in Pyrex. At 5 cm distance from the bottom plane the difference is a factor of 2. The lower $NO(X)$ density in aluminium is due to the decrease in the NO volume production rate associated with the reaction $N(^4S) + O(^3P) + N_2 \rightarrow NO(X) + N_2$, since both $N(^4S)$ and $O(^3P)$ densities are smaller in aluminium. However, near the wall a higher density can be found in aluminium due to the larger NO production from the wall. As already mentioned above, the predicted densities are practically equal at 4 cm distance from the wall considering or not the surface production. In stainless steel similar densities can be found as in aluminium, with the most significant differences only taking place very close to the surface.

The density distributions of the $NO(B^2\Pi)$ state are shown in the fourth row of figure 8. As it occurs with the ground-state $NO(X)$, $NO(B)$ is also created in the reactor via the three body reaction $N(^4S) + O(^3P) + N_2 \rightarrow NO(B) + N_2$. The decrease of both atomic densities from Pyrex to metallic surfaces produces the observed decrease for $NO(B)$. Whereas for Pyrex the $NO(B)$ density decreases from the reactor's entrance to the bottom plane with a factor of about 5, in metallic surfaces this decrease is more pronounced with two orders and three orders of magnitude lower, respectively, in aluminium and in stainless steel. Nevertheless, in a 15 cm width zone around the inlet flow,

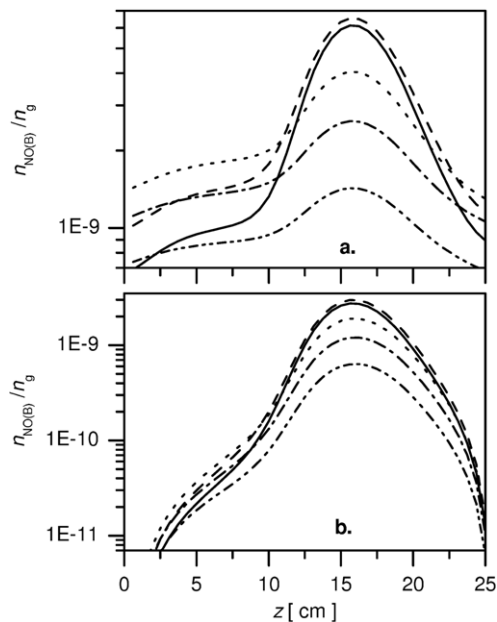


Figure 9. Relative density distribution of $NO(B)$ as a function of z , at $(x, y) = (32.5 \text{ cm}, 12.5 \text{ cm})$ in the case of (a) Pyrex and (b) aluminium surfaces, for the following O_2 percentages: 0.5% (\cdots), 1% ($-\cdot-$), 2% (\cdots), 5% ($- - -$) and 7% ($—$).

roughly from $z = 7.5 \text{ cm}$ to $z = 22.5 \text{ cm}$, the decrease in the $NO(B)$ density in metallic wall reactors, in comparison with that in Pyrex, is only one order of magnitude.

Finally, in the last row of figure 8 the density distributions of O_3 are presented. Here, ozone is mainly created by re-association of $O(^3P)$ atoms and $O_2(X)$ ground-state molecules in the presence of N_2 and $O(^3P)$, that is via the three-body reactions $O(^3P) + O_2(X) + N_2 \rightarrow O_3 + N_2$ and $O(^3P) + O_2(X) + O(^3P) \rightarrow O_3 + O(^3P)$. As, due to the recombination of $O(^3P)$ atoms on the surface into $O_2(X)$, the $O_2(X)$ density increases in the vicinity of the wall, which results in an increase in O_3 density. Accordingly, the O_3 densities near the wall are larger by one order of magnitude in metallic surfaces than in the Pyrex. Moreover, it is worth noting that only minor modifications have been obtained for the O_3 density distribution by varying the assumed α value.

3.4. Influence of O_2 percentage

The results presented so far have been obtained for an N_2 -2% O_2 initial mixture composition. In the following we will discuss briefly the modifications on the predicted density distributions as other O_2 percentages are considered, both for Pyrex and aluminium surfaces. Since the plasma sterilization is attributed mainly to an erosion effect produced by $O(^3P)$ atoms together with a spore inactivation effect of UV photons emitted by $NO(B^2\Pi)$ states, we will choose these two species for illustrating the effects of changing the O_2 percentage. Furthermore, it has been found in [17, 19], by varying the O_2 percentage, that the sterilization efficiency presents a maximum for the conditions at which the UV intensity from NO_β bands is the largest.

Figure 9 shows the density distribution of $NO(B^2\Pi)$ as a function of the z coordinate, that is, as a function of the

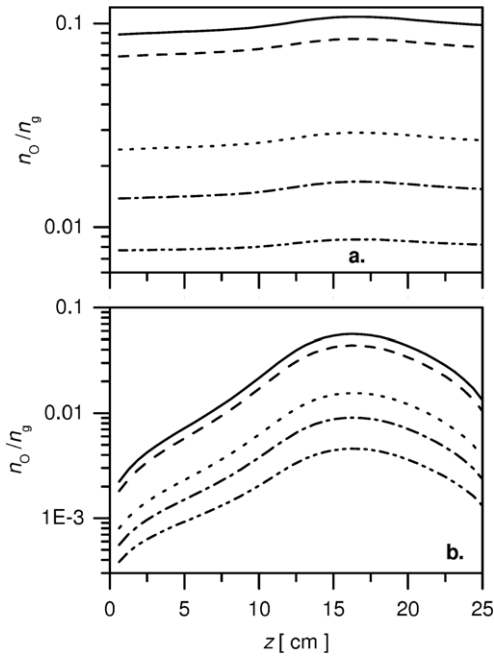


Figure 10. Relative density distribution of O(³P) as a function of z , at $(x, y) = (32.5 \text{ cm}, 12.5 \text{ cm})$ in the case of (a) Pyrex and (b) aluminium surfaces, for the following O₂ percentages: 0.5% (---), 1% (- · - ·), 2% (·····), 5% (- - -) and 7% (—).

vertical coordinate, in a point at the middle of the reactor, $(x, y) = (32.5 \text{ cm}, 12.5 \text{ cm})$, for different O₂ percentages in the range 0.5–7%, in the case of Pyrex and aluminium surfaces. Here, we assume independent γ_N and γ_O probabilities on the added O₂ percentage, with the same values as considered before for 2% of O₂: $\gamma_N = 2 \times 10^{-4}$ and $\gamma_O = 4 \times 10^{-4}$ in Pyrex; $\gamma_N = 2.3 \times 10^{-2}$ and $\gamma_O = 2 \times 10^{-2}$ in aluminium.

In Pyrex, the highest NO(*B*) density is found at the inlet position, $z \sim 15 \text{ cm}$, at 5% of added O₂ with a relative value of $[\text{NO}(B)]/N_g \sim 6.5 \times 10^{-9}$. However, closer to the walls there is a much faster decrease in NO(*B*) concentration as the O₂ percentage increases beyond 1%, as a result of which at $\Delta z \sim 5 \text{ cm}$ away from the entrance, the highest NO(*B*) density occurs at a lower O₂ percentage $\sim 2\%$. At this region also the NO(*B*) density obtained at 7% of O₂ decreases below its corresponding value at 1%, the difference being a factor of 2. The asymmetrical shape of NO(*B*) density shown in figure 9(a) results from the fact that the reactor outlet is positioned on the top plane $z = 25 \text{ cm}$, at $x = 40 \text{ cm}$. In the case of the aluminium surface, the same behaviour is observed in figure 9(b); however, instead of reaching a kind of plateau at $z = 0\text{--}10 \text{ cm}$, the density decrease towards the wall is now much more pronounced. Globally, the NO(*B*) concentration is higher in Pyrex than in aluminium.

The density distribution of O(³P) is presented in figure 10, for the same conditions as in NO(*B*) molecules. In the case of a Pyrex reactor, an almost homogeneous distribution is obtained regardless of the O₂ percentage we consider, see figure 10(a). Furthermore, a nearly linear increase in O(³P) density with O₂ percentage can be identified. On the contrary, in the case of an aluminium reactor, although there is an increase in O(³P) density with O₂ percentage, the density decrease towards the bottom and the top walls, at $z = 0$ and $z = 25 \text{ cm}$, is now

very pronounced due to higher atomic surface losses, see figure 10(b). Results with approximately the same trend as in aluminium are also obtained in stainless steel.

According to these results, concentrations of active species necessary for plasma sterilization, namely, of O(³P) atoms and NO(*B*²Π) states, may exist with all three reactors, for approximately the same conditions. However, the expected sterilization times for a material placed in the reactor close to the bottom should be considerably larger in aluminium and stainless steel than in Pyrex, due to lower concentrations for the two species. Thus, the most efficient sterilization should occur in principle in Pyrex.

4. Conclusions

The effects of surface losses of N(⁴S) and O(³P) atoms on the density distributions of different species in a post-discharge reactor have been investigated using a three-dimensional hydrodynamic model for three different wall materials: (i) Pyrex, (ii) aluminium and (iii) stainless steel. The calculations have been carried out for the case of a $65 \times 25 \times 25 \text{ cm}^3$ post-discharge reactor fed from a 2450 MHz discharge conducted in an N₂-*x*O₂ mixture composition, with $x = 0.5\text{--}7\%$, at 2 Torr and $2 \times 10^3 \text{ sccm}$ flow rate.

We have analysed the influence of increasing the N-atoms surface loss probability on the predicted concentrations of N(⁴S) and O(³P) atoms. It has been found that when the γ_N probability in stainless steel increases by a factor of 10, the concentration of N atoms in the reactor decreases by a factor of 1.6, while in the vicinity of the walls this decrease is larger by a factor of 2.5. Further, the increase in γ_N has no effect on the O-atoms density. With regard to the surface losses of O atoms, it has been seen that the neglect of such processes, in the case of Pyrex reactors, produces a nearly homogeneous increase in the O-atoms density with about 20% in the whole reactor.

The surface losses of N(⁴S) and O(³P) atoms give place not only to recombination into N₂ and O₂ but also to wall production of NO(*X*). The contribution of NO surface production to the increase in the total volume concentration of NO(*X*) in the reactor has been investigated. It has been found that due to the very efficient decomposition reaction $\text{NO}(X) + \text{N}(\text{4S}) \rightarrow \text{N}_2(X, v \simeq 3) + \text{O}(\text{3P})$, at different NO production rates some differences exist only in a narrow 5 cm within the zone near the wall. In the other regions of the reactor no changes are observed independently of the percentage of the atomic surface loss rate we assume to be reconverted to form NO(*X*).

The species densities distributions have also been compared for different wall materials. It has been found that the densities of N(⁴S) and O(³P) atoms, as well as those of NO(*X*) and NO(*B*), decrease from Pyrex to metal. The density of O(³P) atoms in aluminium is lower than in Pyrex by a factor varying between 1.5 and 10, depending on the position in the reactor. In stainless steel the density is still lower with a density decrease of 25 near the bottom of the reactor. In turn, the decrease in N(⁴S) density from Pyrex to metal occurs to a lesser extent than it could be expected from the simple increase in γ_N probability. This happens because of the decrease in the volume loss rate of N atoms associated with the three-body

reaction $N(^4S) + O(^3P) + N_2 \rightarrow NO(X) + N_2$, since the O-atoms density also decreases from one to another material. This reaction produces NO(X), so that the concentration of this species decreases slightly in the volume reactor. A reverse behaviour occurs at the surface, since the rate for NO(X) surface production increases from Pyrex to metal, but this increase takes place only in a narrow region in the vicinity of the wall.

Similarly to NO(X), the upper state NO(B) is also created through a three-body reaction $N(^4S) + O(^3P) + N_2 \rightarrow NO(B) + N_2$, so that the density of this species is also lower in metal than in Pyrex, due to smaller atomic densities. In aluminium the NO(B) density is lower by more than one order of magnitude than in Pyrex, while in stainless steel this difference is by more than two orders of magnitude. The only species whose density increases from Pyrex to metal is ozone. Due to the surface recombination of $O(^3P)$ into O_2 , the rate of O_3 production in the vicinity of the wall increases, which results in higher densities for ozone up to one order of magnitude in the whole reactor.

Finally, it has been seen that the behaviour of NO(B) and $O(^3P)$ densities as a function of the O_2 percentage is independent of the wall's material. Whichever the reactor we consider the highest NO(B) density is found at 5% and 2%, respectively, in the flow direction and in positions outside the gas flow. Obviously, the highest $O(^3P)$ density occurs at the highest O_2 percentage. Consequently, plasma sterilization can occur with all three reactors, but the expected sterilization times may vary a lot from one to another reactor, as well as with the position where the sample to be sterilized is placed.

This model constitutes a first attempt to evaluate the effects of atomic surface losses on the post-discharge reactors used for plasma sterilizations and other applications. Due to the lack of data on the different elementary surface processes involved in heterogeneous catalysis only a parametric study of this type can be realized. In order to improve the accuracy of the model a more detailed description of the surface kinetics is needed but the absence of data for the surface coverage with adsorbed N and O atoms, as a function of N_2 - O_2 mixture composition, as well as for the activation energies, prevents a more detailed study from being conducted. In spite of this weakness the authors believe that this study can be a useful tool to evaluate the extension of surface effects in post-discharge reactors.

Acknowledgments

This work has been supported by the Portuguese Science Foundation FCT through project POCTI/FAT/44221/2002, co-financed by FEDER, and through the post-doctoral fellowship of KK. The authors also wish to acknowledge V Guerra and Z Lj Petrovic for fruitful discussions.

References

- [1] Gaillard M, Raynaud P and Ricard A 1999 *Plasma Polym.* **4** 241
- [2] Moreau S *et al* 2000 *J. Appl. Phys.* **88** 1166
- [3] Ricard A and Monna V 2002 *Plasma Sources Sci. Technol.* **11** 1
- [4] Lin T H, Belser M and Tzeng Y 1988 *IEEE Trans. Plasma Sci.* **16** 631
- [5] Hody V *et al.* 2006 *Thin Solid Films* **506–507** 212
- [6] Yasuda Y, Zaima S, Kaida T and Koide Y 1990 *J. Appl. Phys.* **67** 2603
- [7] Barnes T M *et al* 2004 *J. Appl. Phys.* **96** 7036
- [8] Sage D, Espuche E and Soulier J-P 1999 *Le Vide* **54** 429
- [9] Garnier A *et al* 1994 *J. Appl. Phys.* **75** 104
- [10] Dilecce S and De Benedictis S 1999 *Plasma Sources Sci. Technol.* **8** 266
- [11] Nahorny J *et al* 1995 *J. Phys. D: Appl. Phys.* **28** 738
- [12] Cartry G, Magne L and Cernogora G 1999 *J. Phys. D: Appl. Phys.* **32** 1894
- [13] Gordiets B and Ricard A 1993 *Plasma Sources Sci. Technol.* **2** 158
- [14] Gordiets B, Ferreira C M, Guerra V, Loureiro J, Nahorny J, Pagnon D, Touzeau M and Vialle M 1995 *IEEE Trans. Plasma Sci.* **23** 750
- [15] Guerra V and Loureiro J 1999 *Plasma Sources Sci. Technol.* **8** 110
- [16] Ricard A, Moisan M and Moreau S 2001 *J. Phys. D: Appl. Phys.* **34** 1203
- [17] Philip N, Saoudi B, Crevier M-Ch, Moisan M, Barbeau J and Pelletier J 2002 *IEEE Trans. Plasma Sci.* **30** 1429
- [18] Ricard A, Monna M and Mozetic M 2003 *Surf. Coat. Technol.* **174–175** 905
- [19] Villeger S, Cousty S, Ricard A and Sixou M 2003 *J. Phys. D: Appl. Phys.* **36** L60
- [20] Moisan M, Barbeau J, Crevier M-Ch, Pelletier J, Philip N and Saoudi B 2002 *Pure Appl. Chem.* **74** 349
- [21] Kutasi K, Pintassilgo C D, Coelho P J and Loureiro J 2006 *J. Phys. D: Appl. Phys.* **39** 3978
- [22] Kutasi K, Pintassilgo C D, Loureiro J and Coelho P J 2007 *J. Phys. D: Appl. Phys.* **40** 1990
- [23] Pintassilgo C D, Loureiro J and Guerra V 2005 *J. Phys. D: Appl. Phys.* **38** 417
- [24] Kim Y C and Boudart M 1991 *Langmuir* **7** 2999
- [25] Yamashita T 1979 *J. Chem. Phys.* **70** 4248
- [26] Rahman M L and Linnett J W 1971 *Trans. Faraday Soc.* **67** 170
- [27] Mavroyannis C and Winkler C A 1961 *Can. J. Chem.* **39** 1601
- [28] Sancier K M, Fredericks W J, Hatchett J L and Wise H 1962 *J. Chem. Phys.* **37** 1798
- [29] Gordiets B, Ferreira C M, Nahorny J, Pagnon D, Touzeau M and Vialle M 1996 *J. Phys. D: Appl. Phys.* **29** 1021
- [30] Ricard A, Popescu A, Baltog A and Lungu C P 1996 *Vide Sci. Tech. Appl.* **280** 52 248
- [31] Lefevre L, Belmonte T and Michel H 2000 *J. Appl. Phys.* **87** 7497
- [32] Wickramanayaka S, Hosokawa N and Hatanaka Y 1991 *Japan. J. Appl. Phys.* **30** 2897
- [33] Greaves J C and Linnett J W 1958 *Trans. Faraday Soc.* **54** 1323
- [34] Kaufman F and Kelso J R 1967 *J. Chem. Phys.* **46** 4541
- [35] Morgan J E and Schiff H I 1963 *J. Chem. Phys.* **38** 1495
- [36] Pagnon D, Amorim J, Nahorny J, Touzeau M and Vialle M 1995 *J. Phys. D: Appl. Phys.* **28** 1856
- [37] Sabadil H and Pfau S 1985 *Plasma Chem. Plasma Process.* **5** 67
- [38] Macko P, Veis P and Cernogora G S 2004 *Plasma Sources Sci. Technol.* **13** 251
- [39] Adams S F and Miller T A 2000 *Plasma Sources Sci. Technol.* **9** 1
- [40] Singh H, Coburn J W and Graves D B 2000 *J. Appl. Phys.* **88** 3748
- [41] Gomez S, Steen P G and Graham W G 2002 *Appl. Phys. Lett.* **81** 19
- [42] Mozetič M and Zalar A 2000 *Appl. Surf. Sci.* **158** 263
- [43] Tserepi A D and Miller T A 1995 *J. Appl. Phys.* **77** 505
- [44] Wickramanayaka S, Meikle S, Kobayashi T, Hosokawa N and Hatanaka Y 1991 *J. Vac. Sci. Technol. A* **9** 2999
- [45] Sarrette J P, Rouffet B and Ricard A 2005 *Plasma Process. Polym.* **3** 120
- [46] Kurucz P F, Guha J and Donnelly V M 2005 *J. Chem. Phys.* **109** 20989

-
- [47] Mozetič M 2003 *Thermodynamic Gas Phase* (Ljubljana: DVTS)
- [48] Cvelbar U and Mozetič M 2007 *J. Phys. D: Appl. Phys.* **40** 2300
- [49] Danilychev A V and Apkarian V A 1993 *J. Chem. Phys.* **99** 8617
- [50] Lefevre L, Belmonte T, Czerwiec T, Ricard A and Michel H 1999 *Surf. Coat. Technol.* **116–119** 1244
- [51] Marković V Lj, Petrović Z Lj and Pejović M M 1995 *Japan. J. Appl. Phys.* **34** 2466
- [52] Nasuti F, Barbato M and Bruno C 1996 *J. Thermophys. Heat Transfer* **10** 131